Computers and Electronics in Agriculture 188 (2021) 106362

Contents lists available at ScienceDirect

Computers and Electronics in Agriculture

journal homepage: www.elsevier.com/locate/compag

Original papers

Analysis of the stochastic excursions of tumbling apples

Claire Flemmer [a,*], Huub Bakker [b], Rory Flemmer [c]

[a] School of Built Environment, Massey University, Palmerston North 4410, New Zealand
[b] School of Food and Advanced Technology, Massey University, Palmerston North 4410, New Zealand
[c] Junior Enterprises Limited, Palmerston North 4410, New Zealand

ARTICLE INFO

Keywords:
Apple inspection
Computer vision
Surface coverage
Feature tracking
Stochastic tumbling

ABSTRACT

There are strong economic pressures to improve automated inspection of apples. A considerable difficulty, acknowledged in the literature, but not adequately quantified, is the question of the extent to which the surface of apples, tumbling randomly on rollers, is covered by camera views during inspection.

This work demonstrates a method to measure the roll, pitch and yaw of tumbling apples by tracking features on the skin between succeeding camera images and then to use the measured data to provide precise statistical descriptions of the tumbling process. The method was tested on an image library of four apple varietals; Eve and Granny Smith, which have mostly uniform skin colour, and Royal Gala and Braeburn which have a variegated skin colour. The images included apples that rotated stem-over-calyx (as the starting position) and apples that rotated equatorially for all varietals. The variegated varietals had many more trackable skin features (1,731–2,065 image pairs) than the mono-coloured varietals (238–859 image pairs) and stem-over-calyx rotation produced more tracking image pairs (723–2,065 image pairs) than equatorial rotation (238–2,041 image pairs), because the stem and calyx provided trackable features.

Probability histograms are presented for the normalized incremental rotation in pitch, roll and yaw for each varietal and each direction of initial rotation. Skew-Gaussian distributions are fitted to the probability data to give the mean, standard deviation, skew and mean square error for the pitch, roll and yaw for each of the four varietals in each of two initial orientations (stem-over-calyx and equatorial). These stochastic characterisations can be used in future Monte Carlo simulations to provide precise determination of camera coverage during the inspection of apples tumbling on rollers. This is an important contribution to the field of automated apple inspection.

1. Introduction

In 2017, world apple production was 87.2 million tonnes (FAO Food and Agriculture Organization of the United Nations, 2019) and with such immense production comes the need for it to be graded and inspected in a fast and reliable manner. This can only be achieved using automated systems because manual inspection is slow, costly, unreliable and has poor repeatability (Chopde et al., 2017; Eissa and Khalik, 2012). Automated grading using computer vision (CV) for size, shape and colour is well-developed and commercial grading systems that do this are common (Wilson et al., 2017). However inspecting apples for defects remains a challenge and is largely reliant on a final manual inspection. There are several comprehensive reviews of the CV research in this area (Zhang et al., 2018; Lu and Lu, 2017; Zhang et al., 2014; Ma et al., 2016) and these highlight three main difficulties. Firstly, it is hard for CV systems to distinguish defects from normal apple features (such as the stem and calyx) particularly when the defect is close to these normal features. Secondly, defects are harder to find on apples with a variegated or multi-coloured skin (such as Royal Gala) compared with mono-coloured apples (such as Granny Smith) since defects may be hidden or obscured in the coloured pattern (Sofu et al., 2016). Thirdly, defect detection can only be accurate if the whole surface is inspected for all apple sizes, shapes and surface topographies (Baek et al., 2019).

In packhouses, apples are commonly placed between rotating biconic rollers to make the apple tumble and, ideally, expose the whole surface to cameras in order to achieve whole-surface inspection (Blasco et al., 2017). Baek et al. (2019) note that this exposes only about two-thirds of the surface to the cameras since the border regions near the rotation axis are not seen by the cameras. They show that the addition of mirrors (to simultaneously capture different views of the apple) can increase the

* Corresponding author.
E-mail address: c.l.flemmer@massey.ac.nz (C. Flemmer).

https://doi.org/10.1016/j.compag.2021.106362
Received 29 December 2020; Received in revised form 28 July 2021; Accepted 29 July 2021
Available online 9 August 2021

exposed area but mirrors are impractical in the dirty packhouse environment. Inspection of defects on round steel balls used in bearings presents a similar problem and various 'surface unfolding' mechanisms are used to ensure that the entire surface is viewed (Chen et al., 2016; Wang et al., 2015). This is a somewhat easier task than unfolding the surface of an apple because apple shape is not spherical but is in fact very varied and complex.

Characterization of apple shape using the 12 ideal apple shapes published by the International Board for plant Genetic Resources is important in defining the properties of new apple cultivars (Paulus and Schrevens, 1999). Zhang et al. (2018) note that for a particular cultivar, variations in season, maturity and origin will have an effect on size and shape. Keshavarzpour and Rashidi (2010) describe apples as varying in shapes from oblong spheroid to oblate spheroid depending on the aspect ratio. Other researchers use Fourier descriptors for the apple shape (Paulus and Schrevens, 1999; Currie et al., 2000). However, despite the obvious fact that apple shape varies, very few studies take this into account when investigating CV inspection for defects on the apple. Most investigations simply assume that varying apple shape will ensure that each apple tumbles randomly as it passes beneath cameras and that with sufficient views the whole surface will be inspected (Sadegaonkar and Wagh, 2015). The exception is Baek et al. (2019) who inspect fiducial dots marked on rotating apples viewed in multiple-mirror images and show that while all the dots are found in 78% of their sample (of 101 apples), dots are either missed or counted more than once in the remaining 22% of the sample.

A further common assumption is that the apple will tumble continuously but this is not always true. A very few researchers note problems such as apples sticking in one position (slipping on the rollers) or being over-packed on rollers. Eissa and Khalik (2012) report that apple rotation on rollers is non uniform 'due to differences in apple sizes and frequent bouncing due to non-uniform shapes.' Sofu et al. (2016) note that catching images that define all sides of the apple is difficult because larger apples do not 'easily whirl round' on the rotating rollers. Wilson et al. (2017) mentions the need to track points as they move below several cameras and Zhang et al. (2014) note that whole surface inspection remains one of the challenges for CV inspection of defects. In the context of surface measurement, Leach et al. (2015) discuss the general need to take numerous measurements of small overlapping regions of interest with an accurate recording of the way in which the object is rotated (to ensure that the entire surface is unfolded and seen). However, controlling the rotation may be too time consuming to be practically useful (Zhang et al., 2018). Bakker et al. (2017) provide an analysis of the number of cameras required to inspect the entire surface of a sphere rotating on biconic rollers assuming that there is no slip between the sphere and the rollers. They also provide an analysis of redundancy, i.e. inspecting the surface more than once, which is undesirable since it adds unnecessary overhead to the inspection processing time and may increase the frequency of false positives.

In summary, there is a need for precise measurement of the rolling behaviour of apples to establish the extent to which whole-surface exposure occurs as they tumble. Apples can be positioned so that they rotate initially either stem-over-calyx (SC) or equatorially (EQ). In the general case an apple will rotate on an axis that lies somewhere between these two axes. This investigation considers initial SC and EQ rotation as the two extreme cases and determines the way in which the position of a point of interest on the apple moves for each. Two mono-coloured varietals (Eve and Granny Smith) and two multi-coloured apple varietals (Royal Gala and Braeburn) are tested.

2. Materials and methods

2.1. Experimental data

A detailed description of the experimental rig used to collect the library of apple images used in this work is provided in Caulton (2011). The apples were placed on 65 mm diameter rollers, 92 mm between centres, rotating at 0.5 revolutions per second. Over a period of 2 s the apple moved through one full rotation and each camera captured 30 images (i.e., one image for every 12 degrees of rotation of the apple). High frequency (20 kHz) fluorescent lamps were used for lighting, together with linear Polyvinyl Alcohol-Iodine (LPL) filters to remove specular reflections from the apple skin. The camera was set to auto exposure, with the white rollers ensuring that the apple images were not overexposed.

The camera was mounted 340 mm above the centre of rotation of the apples. The apples varied in size from 62 mm to 100 mm diameter. The library consists of 20,880 images comprised of serial images of 348 apples moving on rotating cylindrical rollers (beneath a camera) with varying degree of pitch, roll and yaw (as defined in Fig. 1) between consecutive images.

The apples are one of four varietals; Eve and Granny Smith which have mostly uniform skin colour (red and green respectively) and Royal Gala and Braeburn which have a variegated skin colour (Fig. 2). The cylindrical rollers are fitted with soft black rubber O-rings with a clear rubber tubing cover. The roller design was chosen during the development of an automated apple packing line (Flemmer et al., 2014) to protect apples from damage as they are dropped onto the roller during the packing process. It differs from the standard biconic roller arrangement but has the advantage that friction between the soft rubber and the apple prevents the apple from slipping during rotation. This ensures precise registration between apple and roller which is desirable in the analysis of tumbling behaviour. The image sequences were captured, at a rate of 15 images per second, for apples rotating stem-over-calyx (SC) and for apples rotating equatorially (EQ). Sample images are shown in Fig. 2.

2.2. Visual tracking analysis

The purpose of visual tracking over several rotations of an apple is to determine the statistical gyrations of real apples in order to estimate how much of the apple surface is seen as it passes under inspection by one or several cameras. In sequential images of a tumbling apple, there is some degree of pitch, roll and yaw, as defined in Fig. 1. The aim is to track a region of interest (ROI), initially near the visual centre of the apple, as it moves from the preceding image to the succeeding image (Fig. 3). The position and rotation of the ROI can be expressed in terms of the corresponding angular incremental changes in pitch, roll and yaw (Fig. 4). The calculation of these incremental changes requires a measure of the distance between the moving surface and the centre of rotation of the apple (i.e., that point in three dimensions that does not move during the interval between acquiring the two images). This

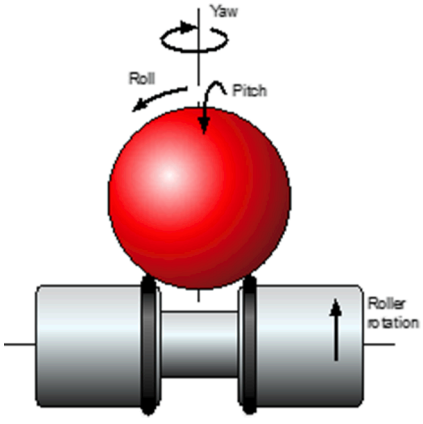

Fig. 1. Set-up of an apple on rollers. The black bands on which the apples rotate are O-rings with clear rubber tubing covering. Rollers rotate clockwise when viewed from the right.

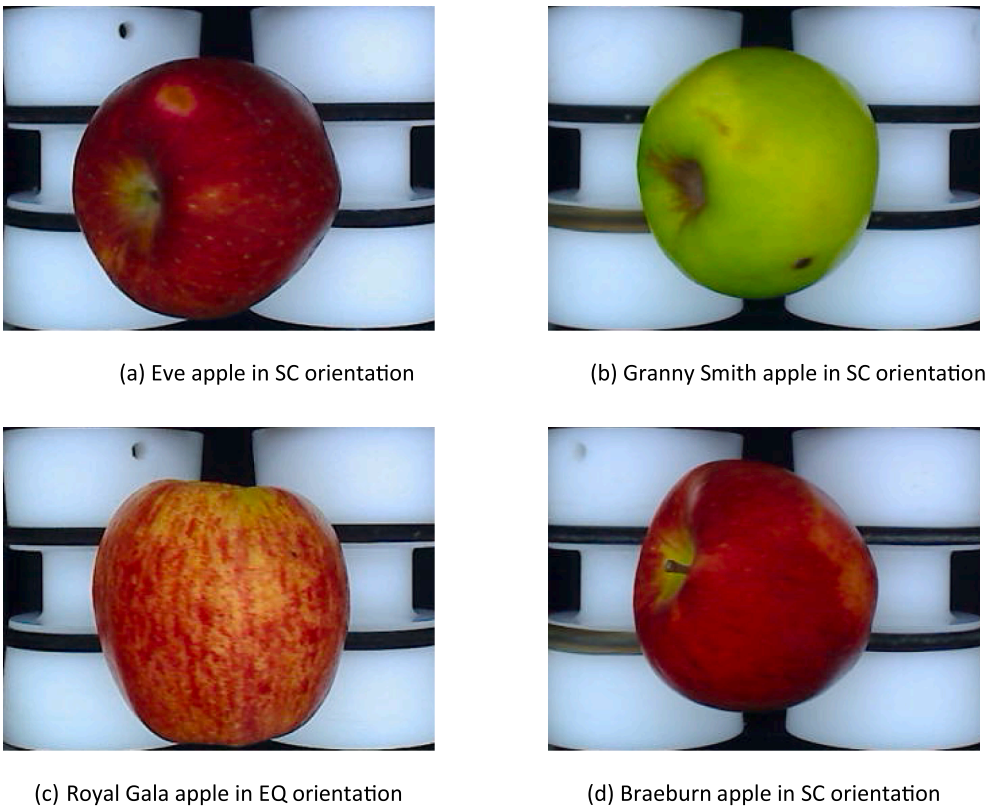

Fig. 2. Sample images showing apple varietals tumbling in one of two orientations. (a) Eve apple in SC orientation, (b) Granny Smith apple in SC orientation, (c) Royal Gala apple in EQ orientation, (d) Braeburn apple in SC orientation.

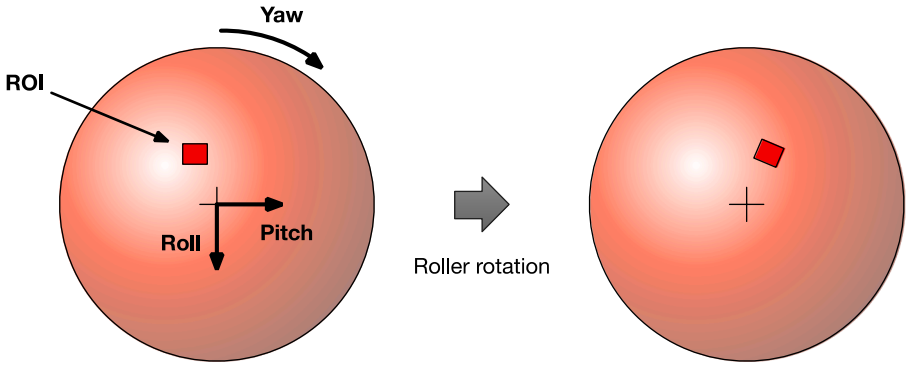

Fig. 3. View from above of movement of a region of interest (ROI) from one image to the next in terms of pitch, roll and yaw rotations.

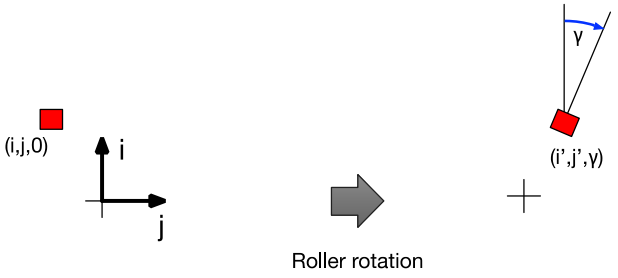

Fig. 4. Coordinate system used in images. The view is vertically downwards, from the camera's pupil.

distance is the instantaneous radius for the rotation, r_s.

We begin with a ROI centred at (i,j) in the first image and with no rotation ($\gamma = 0$), i.e. at starting condition$(i,j,0)$). Note that this notation does not agree with the raster of the camera retina and a simple transformation is necessary before using pixel data. The camera, facing vertically downward, takes an initial image and we identify a region of interest located at i,j in this image. Note that the location of the initial location (i,j) is generally not at the centre of the image. In the second image this ROI has moved to location(i',j',γ). We may view this composite rotation as being comprised of incremental changes in pitch, roll and yaw which we refer to as $\Delta\theta, \Delta\varphi$ and ω respectively and which we assume act about the centre of the apple, which is momentarily fixed in space. The instantaneous radius for this rotation is r_s.

The axis about which the apple pitches is parallel to the axis of the rollers and is represented by a vector aligned with this axis. Its length represents the magnitude of differential pitch. Roll of the apple is like that of an aircraft, and acts about an axis pointing in the direction of motion of the aircraft. From Fig. 3 we can see that roll and pitch are aligned with the cardinal axes, therefore, incremental roll only affects the i-coordinate in the new image while incremental pitch only affects

the j-coordinate. An aircraft or apple yaws when it rotates about a vertical axis and therefore, the yaw, ω, is the same as γ and results in change to both i- and j-coordinates. We will look at these transformations individually; assuming that pitch happens without roll and yaw, roll happens without pitch and yaw and yaw happens without pitch and roll.

2.2.1. Pitch

Fig. 5 shows a view of the apple along the line of the roller. The initial condition is shown in Fig. 5(a), where the location of the centre of the ROI has a coordinate, i.

$$\theta = sin^{-1}\left(i/_{r_s}\right) \tag{1}$$

After a rotation (change in pitch) of $\Delta\theta$ from the initial condition the location of the centre of the ROI has moved to coordinate $i_\theta^{'}$ and we have the situation shown in Fig. 5(b). The change in pitch angle $\Delta\theta$ is:

$$\Delta\theta = \sin^{-1}\left(\frac{i_\theta^{'}}{r_s}\right) - \sin^{-1}\left(\frac{i}{r_s}\right) \tag{2}$$

The change in the position of the point between images is given by:

$$\Delta i = i_\theta^{'} - i \tag{3}$$

Substituting $i_\theta^{'}$ from (3) into (2):

$$\Delta\theta = \sin^{-1}\left(\frac{i+\Delta i}{r_s}\right) - \sin^{-1}\left(\frac{i}{r_s}\right) \tag{4}$$

2.2.2. Roll

By a similar analysis the initial position in the roll direction is given by:

$$\varphi = sin^{-1}\left(\frac{j}{r_s}\right) \tag{5}$$

And the change in roll angle from one image to the next is given by:

$$\Delta\varphi = \sin^{-1}\left(\frac{j+\Delta j}{r_s}\right) - \sin^{-1}\left(\frac{j}{r_s}\right) \tag{6}$$

where j is the initial position on the image, Δj is the displacement between the two images and $\Delta\varphi$ is the angle through which the apple rolls.

2.2.3. Yaw

The effects of yawing the apple are more complex because they affect both i- and j-coordinates. However, this is simplified by the fact that the (pure) yaw angle, ω, is the same as the rotation angle of the ROI between images, γ (Fig. 6). This is because our initial ROI has zero yaw, by definition.

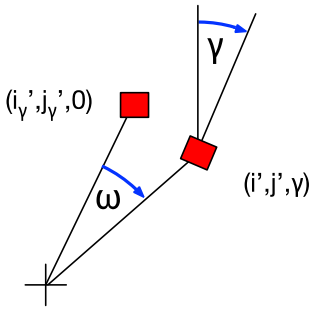

Fig. 6. Position of the ROI that would result in the final position due solely to a yawing movement. Yaw angle, ω, is equal to the rotation of the ROI, γ.

If we define the initial coordinates of the ROI before the yaw rotation as $\left(i_\gamma^{'}, j_\gamma^{'}, 0\right)$ (i.e. oriented with the axes) then a yaw of ω will produce a ROI rotated by γ from the vertical. We will see that the process of mapping (by regression on the data), the initial ROI to the succeeding ROI provides a value of γ.

2.2.4. Regression to determine the rotated position of the ROI

We now examine a regression of the camera data as an initial and a following image are compared, in order to find the final position of the ROI. Conceptually, the template provided by the initial ROI will be translated and rotated across the second image in order to find the best match. This is accomplished by systematically changing the values for i, j and γ and, at each trial location, computing an error function, and assessing how well the template data matches the trial position.

To map a pixel of the initial ROI on the final ROI we can either translate in the i- and j-ordinates and then rotate, or else rotate and then translate. These sets of operations are not commutative. If we choose the former order of operation then the change in the coordinates, Δi and Δj, will be known to us as outputs of the regression algorithm. This is also true of the rotation angle, γ. This is shown in Fig. 7 where the output of the regression operation will be the triplet of $\Delta i_\theta, \Delta j_\varphi, \gamma$.

From this parameter triplet we can directly calculate the pitch, roll and yaw angles using the equations from the previous sections and the apple radius, r_s, whose value we now consider.

2.2.5. Effective apple radius

To perform the above calculations, we must use a value for r_s, the effective radius of the apple. By Euler's Theorem, for any general rotation, from an initial orientation to a final orientation, there exists a fixed line in three-space about which the object rotates from initial to final configuration. The shortest distance from this line to either of the ROIs is

(a) Initial position and pitch angle of ROI

(b) Position and angle of ROI after incremental change in pitch

Fig. 5. Apple rotation due to change in pitch about radius r_s. (a) Initial position and pitch angle of ROI, (b Position and angle of ROI after incremental change in pitch).

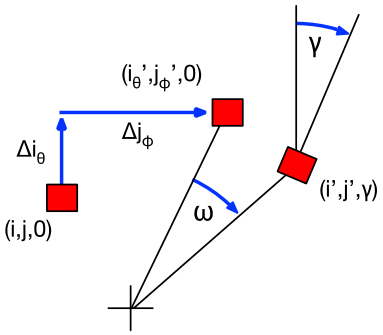

Fig. 7. Consecutive transforms of the ROI from first image to second image.

the effective radius of rotation. The radius of the apple at the rollers determines the angle of rotation for a given change in *i*- and *j*-co-ordinates. Looking at the plan-form profile of an apple as it moves on the rotating rollers (Fig. 8) there are two radii, r_{upper} and r_{lower}, which affect the rotational behavior of the apple. If the two radii are equal then the apple will rotate only about the pitch axis. If the two radii are different then the apple will rotate in three dimensions with changes in roll and yaw angles as well as in pitch angle. The ratio of the two radii is an indication of their relative difference and the greater this ratio differs from one, the greater the three dimensional rotation. The effective radius, r_s, was assumed to be the average of the upper and lower radii.

2.2.6. Normalisation

If the rollers were biconic, the angular rotation of the rollers would be directly related to the angular rotation of the apple and we would be safe in using the measured pitch, roll and yaw angles directly. However, in this work, the rollers are parallel so that the circumferential distance that the roller rotates is the same as the circumferential distance the apple rotates. This means that the amount of pitch rotation will depend on the apple size. The larger the apple, the smaller will be the pitch rotation. Therefore, we must normalise the angles that we report to eliminate the effect of apple size. This can be done by dividing each of the pitch, roll and yaw angles by the mean pitch angle for all images from one apple.

We must also recognise that the rotation of the apple is a dynamic process and that, unless the rotation is so slow that the apple maintains contact with both rollers at every point, the apple's average movement is dependent on the rate of rotation of the rollers and cannot be reported independent of this. The amount of rotation between images therefore provides us not with the apples' rotation between those points in time but rather with its angular velocity.

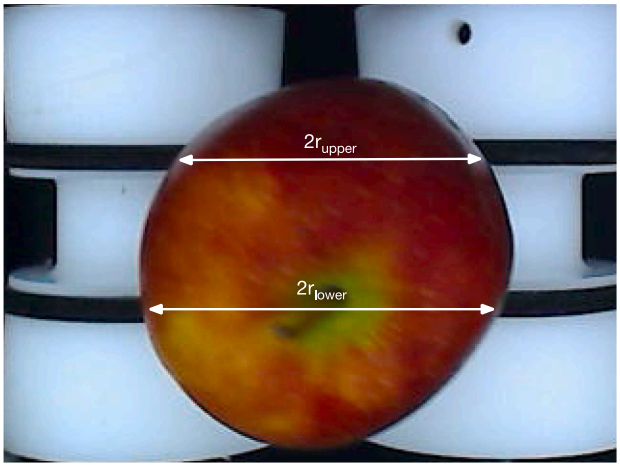

Fig. 8. Apple image showing the definition of the upper and lower horizontal apple radii.

2.2.7. Tracking regions of interest

In any first image (before incremental rotation), three ROIs were defined, each being 50 × 30 pixels in size. The left border of the first ROI was centred on the apple centre and the other two ROIs were positioned 20 pixels above and 20 pixels below the first ROI (Fig. 9). The pixel variability of the three ROIs was assessed and those ROIs that were too bland (i.e. lacking features) were discarded. Mono-coloured apple varietals (particularly Granny Smith) had relatively few qualifying ROIs while Royal Gala apples (with highly patterned skin) had many qualifying ROIs.

In the second image (after the incremental rotation), regression was used to find the translation and rotation with the best fit, as follows:

S1. In the search, each ROI in the first image was conceptually overlaid with its centre on some point on the second image and rotated by some yaw angle.
S2. An objective function was defined by finding the normalised Root Mean Square Error, RMSE, (pixel by pixel) between the pixels in the initial ROI and the pixels in the second image over which the initial ROI was laid.
S3. A Nelder and Mead (1965) algorithm was used to regress for the best fit of each of the qualifying ROIs. Only satisfactory fits were accepted and not all apples yielded data for every transition.
S4. The effective radius of the apple, r_s , was determined as described in Section 2.2.5.
S5. The yaw angle, γ, was determined from the angle of rotation of the ROI as given by the regression.
S6. The pitch and roll angles could then be determined from the Δi and Δj used in the regression algorithm using Eqs. (4) and (6) respectively.
S7. The data were stored, indexed to the apple reference number, frame number and whether the initial orientation was SC or EQ.

The algorithm for obtaining tracking data is summarised in Fig. 10.

2.2.8. Post processing

The post-processing algorithm is shown in Fig. 11. The threshold RMSE was determined by sorting the image pairs for each varietal and orientation by increasing RMSE. The tracked ROIs were then manually examined to define the RMSE cut-off point representing reliable tracking. The number of accepted image pairs, compared with the total number of image pairs, indicates how many fell within the required limits and were used in subsequent analysis. These quantities are shown in Table 1.

Granny Smith apples have very few features on the almost uniform green skin (Fig. 2) so there are fewer accepted pairs of images where ROIs are tracked. This is most pronounced when the apple is rotated equatorially; only 9% of the image pairs (or 238 image pairs) allow reliable tracking. When Granny Smith apples are rotated stem-over-calyx (SC), 32% of the image pairs (859 image pairs) allow reliable

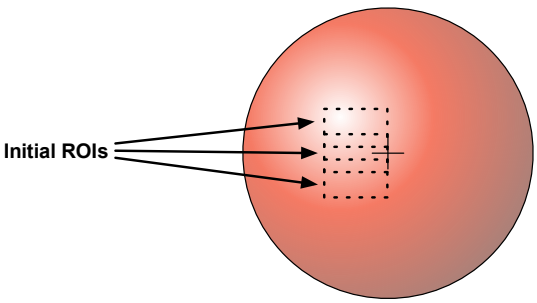

Fig. 9. Three initial regions of interest used for regression.

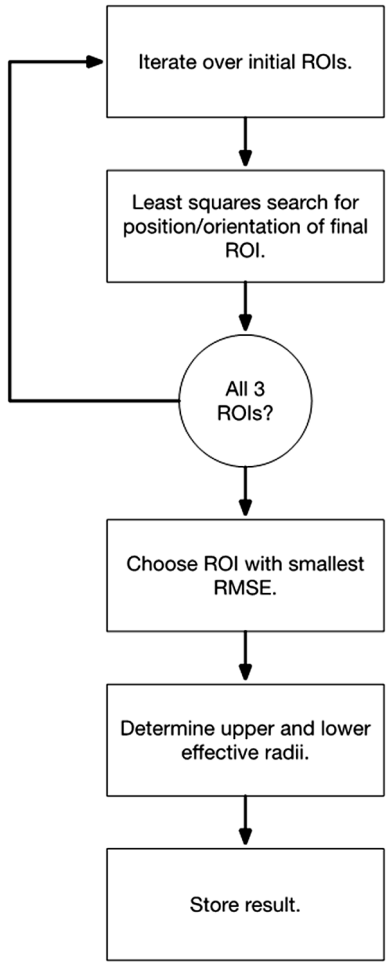

Fig. 10. Method of obtaining tracking data from image pairs for one apple.

tracking because there are more well-defined features in the stem and calyx regions. Eve apples, although largely red in colour, have light speckling on the skin so that a higher percentage of image pairs have trackable ROIs compared with Granny Smith apples. As expected, the highly patterned skin of the Royal Gala varietal (red/yellow variegation with marked striping) is the easiest to track with over 90% of image pairs allowing reliable tracking for both EQ and SC orientations. Braeburn is less variegated with 60% and 37% of image pairs allowing reliable tracking for SC and EQ orientations respectively.

An example of the tracking analysis is shown in Fig. 12 for a Royal Gala apple with initial EQ orientation. The yellow lines show the identification of the boundaries of the apple used to determine the mid-point of the apple (and hence the search area for ROIs). The values for r_{upper} and r_{lower} were found with a template match based on colour transition and were used to calculate the effective radius, r_s. The white rectangle shows the ROI in the left image and, after having undergone a transformation through the three rotation angles, in the right image. The black circle shows the mid-point of the apple plan view. The transformation, in this image pair, can be seen as an almost horizontal shift in the ROI of about 25 pixels to the right with a slight rotation counter clockwise. The accuracy of the tracking process is clearly very much more subtle than could be achieved by human inspection on an industrial packing line.

Although this analysis takes minutes on a modern computer, this is not a problem because such an analysis would only ever be done off-line.

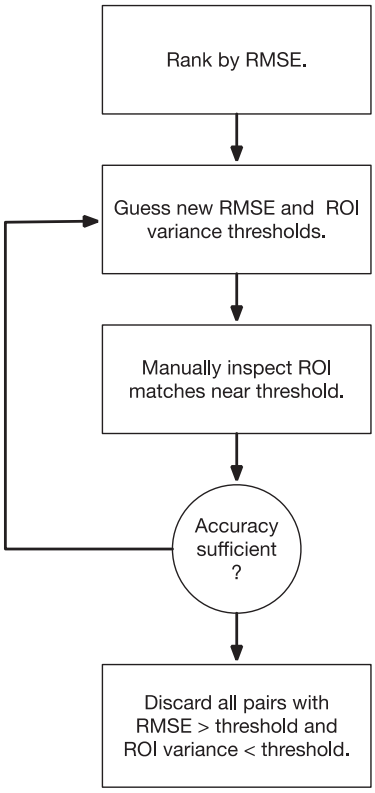

Fig. 11. Method of finding suitable thresholds for selecting acceptable tracking data.

Table 1
The percentage ROI successfully tracked in image pairs for each apple varietal and initial apple orientation.

Varietal	Initial Orientation	Accepted Pairs	Total Pairs	Tracked Pairs (%)
Eve	SC	723	2233	32
Eve	EQ	347	2233	16
Granny Smith	SC	859	2755	32
Granny Smith	EQ	238	2755	9
Royal Gala	SC	2065	2233	92
Royal Gala	EQ	2041	2233	91
Braeburn	SC	1731	2871	60
Braeburn	EQ	1055	2871	37

3. Results and discussion

3.1. Rotation angle variation

The pitch, roll and yaw differential angles between succeeding matched images is shown on box-and-whisker plots (Fig. 13). These are normalised by dividing by the mean differential-pitch angle for each apple.

In these plots, the top and bottom of the boxes represent the upper and lower quartiles, the ends of the whiskers represent local maximum and local minimum, the horizontal line in the boxes is the median, and the red crosses are considered outliers, i.e., outside the local extrema. The local maximum is the last data point that lies within 1.5 times the inter-quartile distance above the upper quartile. The local minimum is the last data point that lies within 1.5 times the inter-quartile distance below the lower quartile. This means that the length of the upper and lower whiskers may not be the same. Although the percentage of matches for some varietals is not high (Table 1), there are between 347

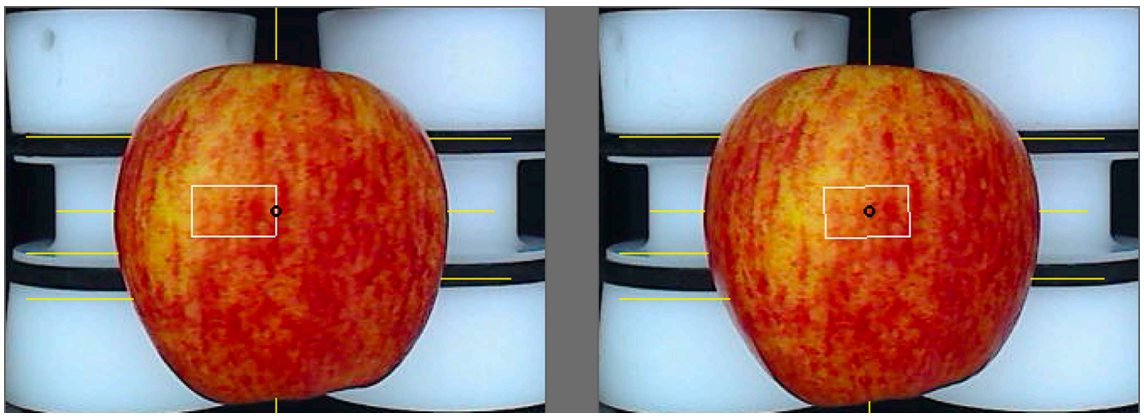

Fig. 12. Analysis of a pair of images for a Royal Gala apple with initial EQ orientation.

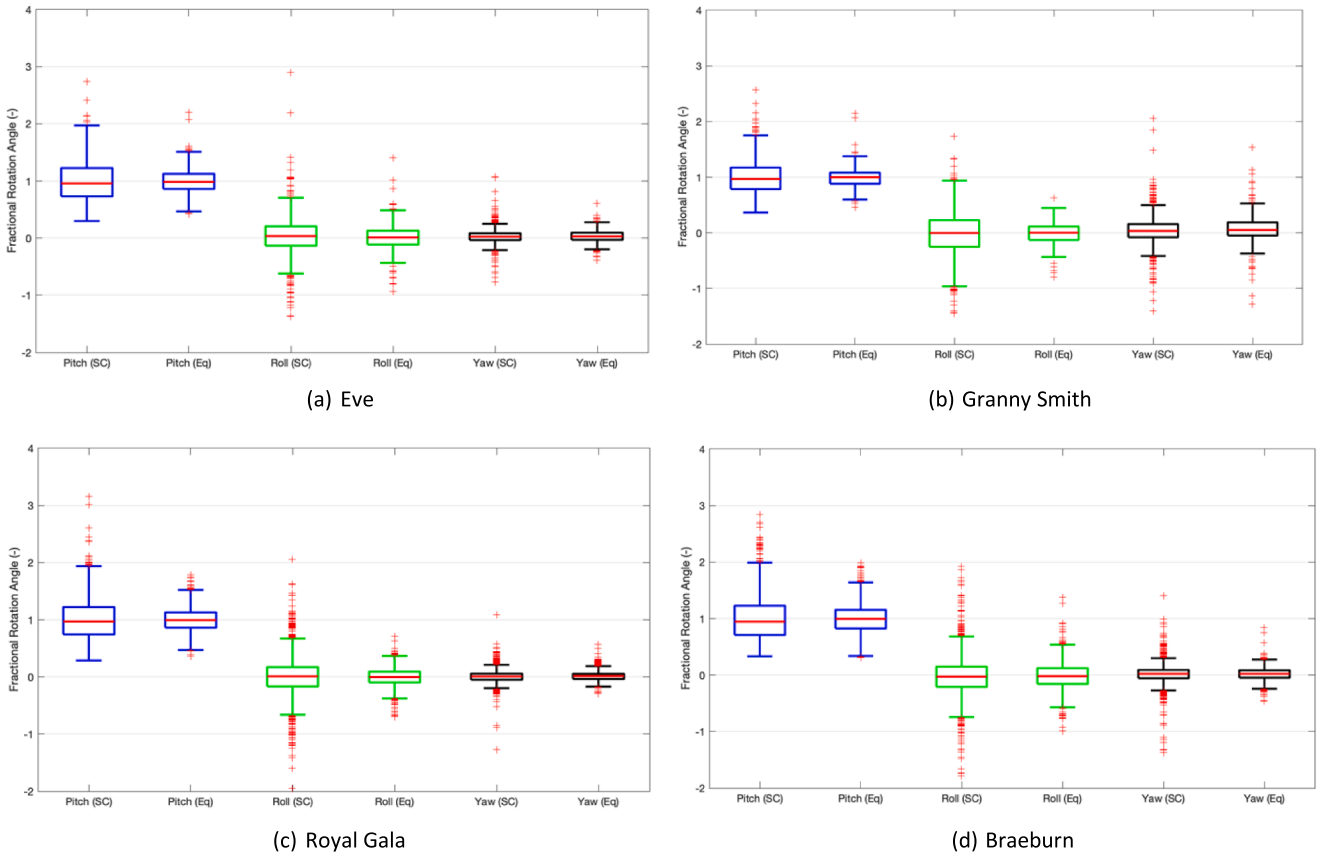

Fig. 13. Distribution of the pitch, roll and yaw differential angles for SC and EQ rotation for each varietal. (a) Eve, (b) Granny Smith, (c) Royal Gala, (d) Braeburn.

and 2,065 matched images for the four varietals, which is large enough that the statistical values of pitch, roll and yaw differentials are meaningful.

3.2. Validation of the apple effective radius

Fig. 14 shows a box-and-whisker plot of all the upper and lower radii measured in the 5,742 images of Braeburn apples (whether they had matched ROIs or not). All radius measurements larger than the box-and-whisker limit (the red crosses on Fig. 14) were discarded, together with any matched ROIs corresponding to these outliers. Although it seems that there are very many red crosses, it must be borne in mind that the box-and-whisker plots represents 1,731 measurements for SC rotation and 1,055 measurements for EQ rotation, so that, overall, the radius measurement is very good. Also shown on Fig. 14 is the ratio of the two radii, expressed as a percentage, for both SC and EQ rotations. The greater the excursion of the ratio from 100%, the greater the rotation of the apple. The plot is shown only for the Braeburn varietal because the other varietals performed similarly.

3.3. Statistical findings

Fig. 15 shows the probability histograms for normalised incremental rotation in the pitch, roll and yaw directions for each varietal for each initial orientation (SC and EQ). The probability is found by dividing the number of observations in each bin by the total number of observations for that varietal. Note that the probability represented in Fig. 15 and tabulated in Tables 2 through 5 are the probabilities of a point lying in

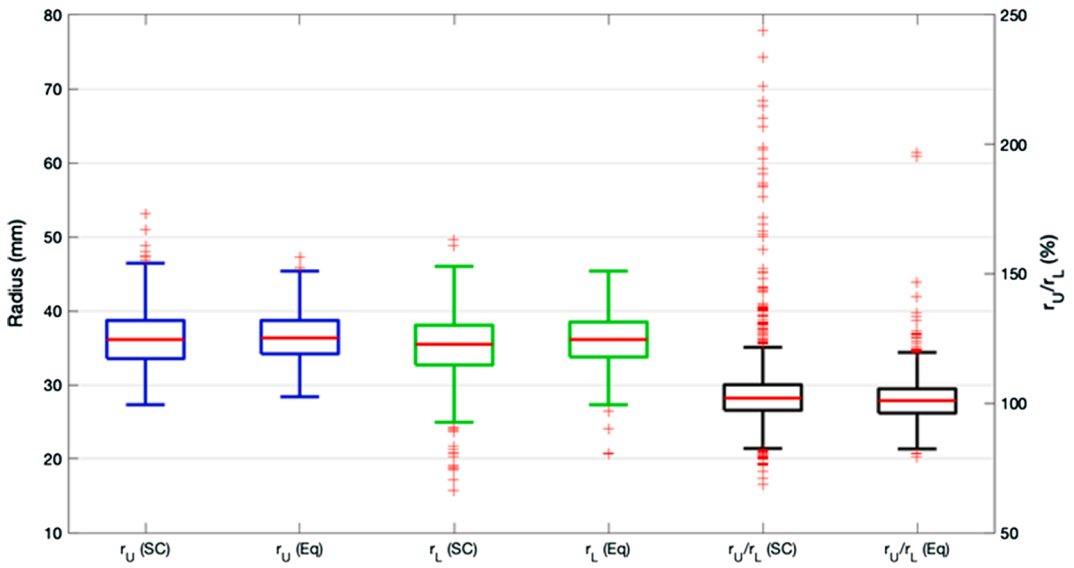

Fig. 14. Braeburn varietal variation in upper radius, r_U, lower radius, r_L, and the ratio of upper radius to lower radius for SC and EQ rotation.

one of the equally spaced bins. This resolution is adequate for a future Monte Carlo simulation.

Skew-Gaussian distributions were fitted to the probability data for each varietal, rotation direction and orientation. The equations are:

$$x' = \frac{x - \bar{x}}{\sigma} \tag{7}$$

$$y = \frac{e^{-1/2x'^2}}{\sigma\sqrt{\pi}} f(s) \tag{8}$$

where x is the independent variable, $\bar{x}$ is the mean, x' is the normalised variable, σ is the standard deviation and $f(s)$ is a piecewise function for the skewness developed by Ashour and Abdel-hameed (2010).

The sum of the probabilities was constrained, during fitting, to be 1 $\pm$ 0.03. The parameters of the fitted distributions are shown in Tables 2–5. These parameters could be used, for example in a Monte Carlo simulation, to replicate the stochastic rolling behaviour of the varietals. The Mean Square Error (MSE) of the fit is shown for incremental pitch, roll and yaw angles in each case.

The results (Fig. 15 and Tables 2 through 5) show:

- For all varietals, the probability distributions of incremental rotation in the pitch, roll and yaw are narrower (have smaller standard deviation) for apples rotating about an initial EQ axis (Fig. 15 b, d, f and h) compared with apples rotating about an initial SC axis (Fig. 15 a, c, e and g). This is expected since rotation about the SC axis is made more irregular by the change in apple shape in the stem-calyx regions.
- For apples rotating about an initial EQ initial orientation, the probability distribution of incremental change in pitch has a varying degree of skew and this affects the value of the mean pitch for the distribution.
- For apples rotating about an initial SC orientation, the skew in the incremental pitch distribution is much higher than for EQ rotation.
- For all varietals rotating about both an initial EQ orientation and an initial SC orientation the normalized incremental distributions are centred approximately on unity for pitch angle and on zero for roll and yaw (Fig. 15 a-h).
- For all varietals and for both initial orientations, roll has a wider variation (standard deviation) than yaw. This was to be expected because any change in yaw is always the result of differential perturbations between the two rollers and we might expect that each perturbation would tend towards the mean, thus providing a smaller yaw – which we see. The single exception is Granny Smith apples with an initial EQ orientation where the variation in incremental roll and yaw is approximately equal (Table 3), indicating that the equatorial region for this varietal is close to spherical.
- The similarity of the curves (Fig. 15 a-h) suggests that an average of these curves might be used for all varietals in order to predict camera coverage, but this will be determined more precisely in future work.

4. Conclusion

Automated inspection of apples using computer vision relies upon the premise that the entire surface of the apple is seen by the cameras as the apple tumbles past. The apples are assumed to tumble in a uniform manner, neither bouncing nor stick-slipping on the rollers and this assumption is held to be true for all apple sizes, shapes and varietals. Whilst researchers have reported seeing irregular tumbling behaviour, no attempt has been made to quantify the extent of irregular rotation and this is the research gap addressed here.

As a first step towards quantifying apple rotation, this research develops a method to obtain a statistically reliable measure of the distribution of rates of pitch, roll and yaw for tumbling apples that is standardised so as to be independent of the apple size and roller speed. The method tracks features on the apple skin in consecutive images of tumbling apples and uses regression to determine the translation and rotation of the features from one image to the next. This allows the incremental changes in three-dimensional rotation (expressed as pitch, roll and yaw angles) to be calculated. These are normalized and used to produce probability histograms of incremental change in pitch, roll and yaw angles that are independent of apple size. Skew-Gaussian distributions are fitted to the histograms to determine the parameters (mean, standard deviation, skew and mean square error) of the changes in pitch, roll and yaw angles of tumbling apples.

The method was applied to an image library of four varietals of apples rotating on non-slip cylindrical rollers. Two of the varietals, Eve and Granny Smith, have mostly mono-coloured skin and the other two varietals, Royal Gala and Braeburn, have multi-coloured/patterned skin. The tracking is significantly easier for multi-coloured varietals than for mono-coloured varietals since the former have many more discernible features than the latter. The images were captured with the apples placed in each of two initial orientations; with rotation stem-over-calyx and equatorially. Rotation stem-over-calyx axis provides more trackable features than rotation equatorially axis because the stem and calyx

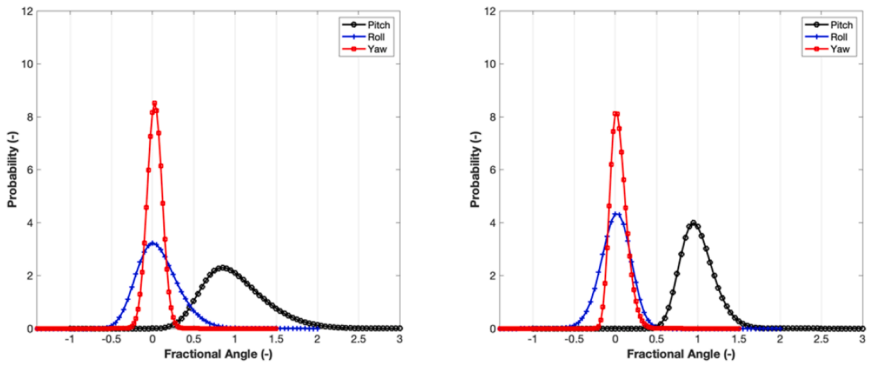

(a) Eve SC initial orientation

(b) Eve EQ initial orientation

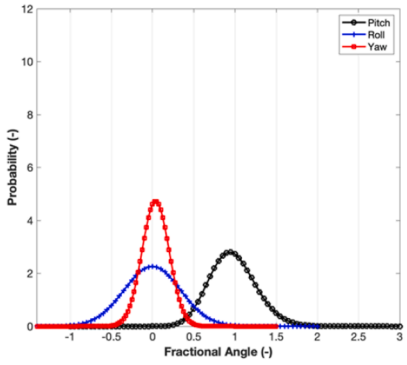

(c) Granny Smith SC initial orientation

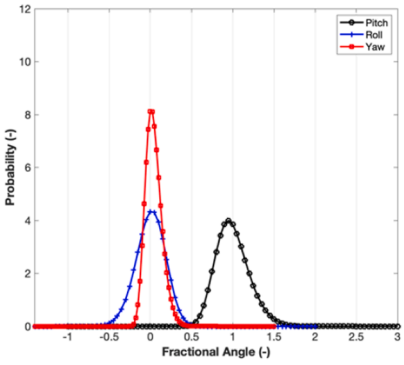

(d) Granny Smith EQ initial orientation

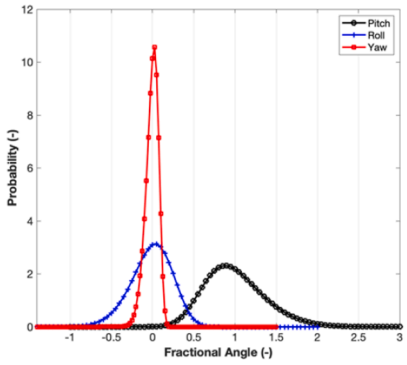

(e) Royal Gala SCinitial orientation

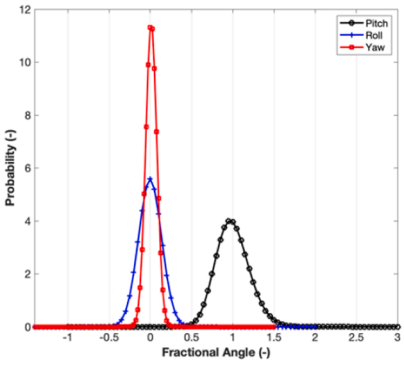

(f) Royal Gala EQ initial orientation

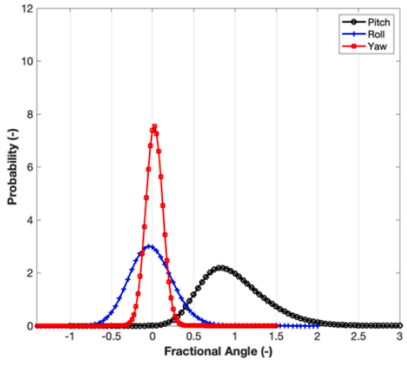

(g) Braeburn SC initial orientation

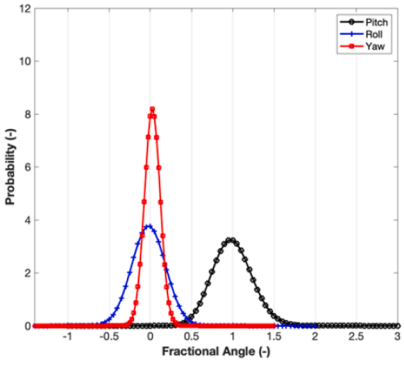

(h) Braeburn EQ initial orientation

Fig. 15. Probability histograms of the incremental angular pitch, roll and yaw between images for the four varietals during rotation. (a) Eve SC initial orientation, (b) Eve EQ initial orientation, (c) Granny Smith SC initial orientation, (d) Granny Smith EQ initial orientation, (e) Royal Gala SCinitial orientation, (f) Royal Gala EQ initial orientation, (g) Braeburn SC initial orientation, (h) Braeburn EQ initial orientation.

Table 2
Skew-Gaussian parameters for the incremental rotation of the Eve varietal in SC and EQ orientation.

	SC Initial Orientation				EQ Initial Orientation			
	Mean	Standard Deviation	Skew	MSE	Mean	Standard Deviation	Skew	MSE
Pitch	0.57	0.58	2.91	0.26	0.79	0.29	2.06	0.43
Roll	−0.19	0.36	2.07	0.38	0.14	0.23	−1.23	0.26
Yaw	0.03	0.09	0.00	0.65	−0.06	0.15	2.31	0.63

Table 3
Skew-Gaussian parameters for the incremental rotation of the Granny Smith varietal in SC and EQ orientation.

	SC Initial Orientation				EQ Initial Orientation			
	Mean	Standard Deviation	Skew	MSE	Mean	Standard Deviation	Skew	MSE
Pitch	0.73	0.37	1.44	0.18	0.99	0.16	0.00	1.88
Roll	0.02	0.34	−0.10	0.30	0.12	0.21	−1.13	0.25
Yaw	0.03	0.16	0.08	0.61	−0.09	0.26	3.63	1.20

Table 4
Skew-Gaussian parameters for the incremental rotation of the Royal Gala varietal in in SC and EQ orientation.

	SC Initial Orientation				EQ Initial Orientation			
	Mean	Standard Deviation	Skew	MSE	Mean	Standard Deviation	Skew	MSE
Pitch	0.60	0.54	2.42	0.18	0.82	0.27	1.55	0.13
Roll	0.23	0.35	−1.78	0.32	−0.01	0.14	0.09	0.09
Yaw	0.08	0.12	−2.71	0.75	0.01	0.07	0.00	1.26

Table 5
Skew-Gaussian parameters for the incremental rotation of the Braeburn varietal in SC and EQ orientation.

	SC Initial Orientation				EQ Initial Orientation			
	Mean	Standard Deviation	Skew	MSE	Mean	Standard Deviation	Skew	MSE
Pitch	0.54	0.59	2.80	0.43	0.82	0.30	1.13	0.13
Roll	−0.21	0.32	1.18	0.37	−0.05	0.21	0.22	0.21
Yaw	0.04	0.10	−0.20	0.58	0.02	0.09	0.00	0.52

regions have distinct features, even on mono-coloured varietals.

In future work, these results can be used in Monte Carlo simulation to determine the extent of apple surface seen by overhead cameras during tumbling. A limitation of the current research is the type of roller, namely non-slip cylindrical. In apple packhouses, biconic rollers are more common. Therefore, the future work will include gathering an image library of apples rotating on biconic rollers and the application of this method to determining the stochastic tumbling behaviour.

Declaration of Competing Interest

The authors declare that they have no known competing financial interests or personal relationships that could have appeared to influence the work reported in this paper.

References

Ashour, S.K., Abdel-hameed, M.A., 2010. Approximate skew normal distribution. J. Adv. Res. 1 (4), 341–350.

Baek, I., Cho, B.-K., Gadsden, S.A., Eggleton, C., Oh, M., Mo, C., Kim, M.S., 2019. A novel hyperspectral line-scan imaging method for whole surfaces of round shaped agricultural products. Biosyst. Eng. 188, 57–66.

Bakker, H.H., Flemmer, R.C., Flemmer, C.L., 2017. Coverage of apple surface for adequate machine vision inspection. In: 24th International Conference on Mechatronics and Machine Vision in Practice (M2VIP), Albany, New Zealand, 23-26 November, 2017. pp. 1-5. IEEE 978-1-5090-6546-2/17 available at: http://ieeexplore.ieee.org/search/searchresult.jsp?queryText=m2vip&refinements=4222234948&refinements=4219132671.

Blasco J., Munera S., Aleixos N., Cubero S., Molto E., 2017. Machine vision-based measurement systems for fruit and vegetable quality control in postharvest. In: Hitzmann, B. (eds) Measurement, Modeling and Automation in Advanced Food Processing. Adv. Biochem. Eng. Biotech, vol. 161, Springer, Cham, 71–91. https://doi.org/10.1007/10_2016_51.

Caulton, M., 2011. An investigation into apple inspection in colour space. Master's thesis. Massey University, New Zealand, pp. 1–85.

Chen, Y.J., Tsai, J.C., Hsu, Y.C., 2016. A real-time surface inspection system for precision steel balls based on machine vision. Meas. Sci. Technol. 27 (7), 074010. https://doi.org/10.1088/0957-0233/27/7/074010.

Chopde, S., Patil, M., Shaikh, A., Chavhan, B., Deshmukh, M., 2017. Developments in computer vision system, focusing on its applications in quality inspection of fruits and vegetables - a review. Agric. Rev. 38 (2), 94–102.

Currie, A.J., Ganeshanandam, S., Noiton, D.A., Garrick, D., Shelbourne, C.J.A., Oraguzie, N., 2000. Quantitative evaluation of apple (*Malus* x *domestica* Borkh.) fruit shape by principal component analysis of Fourier descriptors. Euphytica. 111, 219–227.

Eissa, A.H.A., Khalik, A.A.A., 2012. Understanding color image processing by machine vision for biological materials. Chapter 10. In: Eissa, A.A. (Ed.) Structure and Function of Food Engineering, Intek, pp. 227–274, https://doi.org/10.5772/50796.

Flemmer, R.C., Flemmer, C.L., Caulton, M.J., 2014. Fast apple inspection in colour space. Int. J. Postharvest Tech. Innov. 4 (2–4), 164–177.

Keshavarzpour, F., Rashidi, M., 2010. Classification of apple size and shape based on mass and outer dimensions. American-Eurasian J. Agric. Environ. Sci. 9 (6), 618–621.

Leach, R., Evans, C., He, L., Davies, A., Duparre, A., Henning, A., Jones, C.W., O'Connor, D., 2015. Open questions in surface topography measurement: a roadmap. Surface Topogr.: Metrol. Prop. 3 (1), 1–18.

Lu, Y., Lu, R., 2017. Non-destructive defect detection of apples by spectroscopic and imaging technologies: A review. Trans. Amer. Soc. Agric. Biol. Eng. (ASABE) 60 (5), 1–26.

Ma, J., Sun, D.W., Qu, J.H., Liu, D., Pu, H., Gao, W.H., Zeng, X.A., 2016. Applications of computer vision for assessing quality of agri-food products: a review of recent research advances. Crit. Rev. Food Sci. Nutrit. 56 (1), 113–127. https://doi.org/10.1080/10408398.2013.873885.

Nelder, J.A., Mead, R., 1965. A simplex method for function minimization. Comp. J. 7 (4), 308–313.

Paulus, I., Schrevens, E., 1999. Shape characterization of new apple cultivars by Fourier expansion of digitized images. J. Agric. Eng. Res. 72 (2), 113–118.

Sadegaonkar, V.D., Wagh, K.H., 2015. Automatic sorting using computer vision and image processing for improving apple quality. Int. J. Innov. Res. Dev. 4 (1), 11–14.
Sofu, M.M., Er, O., Kayacan, M.C., Cetişli, B., 2016. Design of an automatic apple sorting system using machine vision. Comput. Electron. Agric. 127, 395–405.
FAO (Food and Agriculture Organization of the United Nations), 2019. Apple production statistics. Available from http://www.fao.org/faostat/en/#data/QC (accessed 5 August 2021).
Wang, Z., Xing, Q., Fu, L., Sun, H. Realtime vision-based surface defect inspection of steel balls. Trans. Tianjin Univ. 21(1), 76–82, DOI 10.1007/s12209-015-2452-6.
Wilson, A., Ben-Tal, G., Heather, J., Oliver, R., Valkenburg, R., 2017. Calibrating cameras in an industrial produce inspection system. Comput. Electron. Agric. 140, 386–396.
Zhang, B., Huang, W., Li, J., Zhao, C., Fan, S., Wu, J., Liu, C., 2014. Principles, developments and applications of computer vision for external quality inspection of fruits and vegetables: a review. Food Res. Int. 62, 326–343.
Zhang, B., Gu, B., Tian, G., Zhou, J., Huang, J., Xiong, Y., 2018. Challenges and solutions of optical-based nondestructive quality inspection for robotic fruit and vegetable grading systems: a technical review. Trends Food Sci. Tech. 81, 213–231.